

Direct Immunofluorescence of Plant Microtubules Based on Semiconductor Nanocrystals

K. Eggenberger,[†] A. Merkulov,[‡] M. Darbandi,[‡] T. Nann,^{‡,§} and P. Nick^{*,†}

Institut of Botany 1, University of Karlsruhe, Kaiserstrasse 2, D-76128 Karlsruhe, Germany, Freiburg Materials Research Centre, University of Freiburg, Stefan-Meier-Strasse 21, D-79104 Freiburg, Germany, and School of Chemical Sciences and Pharmacy, University of East Anglia (UEA), Norwich NR4 7TJ, U.K. Received May 25, 2007

Fluorescence microscopy in combination with multiple, simultaneous labeling of biomolecules has been a key breakthrough in cell biology. However, the spatiotemporal resolution of this approach is limited by bleaching of the fluorescence label and illegitimate cross-reference of the label. CdSe-based semiconductor nanocrystals with their excellent bleaching stability would be an alternative to overcome this limitation. We therefore explored direct immunofluorescence based on nanocrystal-conjugated antibodies using plant microtubules as model. We compared two strategies of bioconjugation, covalent coupling of antitubulin antibodies to BSA-coated nanocrystals and covalent coupling to nanocrystals that were surrounded by functionalized silica shells. Both nanoparticle–antibody conjugates were used to follow the dynamic reorganization of microtubules through the cell cycle of a tobacco cell culture in double and triple staining with FITC as conventional fluorochrome and Hoechst 33258 as marker for mitotic duplication of DNA. BSA-coated nanocrystals visualized fluorescent dots that decorated the various arrays of microtubules. The specificity of the antibody was maintained after conjugation with the nanocrystals, and the antibodies correctly represented the dynamics of cell-cycle-dependent microtubular reorganization. However, this approach did not yield a contiguous signal. In contrast, silica-shelled nanocrystals visualized contiguous microtubules in the same pattern as found for the conventional fluorochrome FITC and thus can be used as labels for direct immunofluorescence in plant cells.

INTRODUCTION

Luminescent semiconductor nanocrystals with spherical morphology (so called quantum dots or QDs¹) have attracted enormous interest as labels for bioimaging (for recent reviews, see refs 1 and 2) because of their increased fluorescence intensity and bleaching resistance. In addition, they can be excited over a broad wavelength range but emit with a narrow band that can be tuned by the size of the particles. Thus, QDs are endowed with optical properties that renders them superior over the organic fluorophores that are used conventionally. However, the application of QDs for cell biology is limited by their potential cytotoxicity (which is discussed controversially (3–6)), their large size (2), and the challenging task to stabilize those nanoparticles colloidally under the general conditions of biological applications.

To overcome these limitations, QDs have been coated with inert silica shells or, alternatively, by thin layers of organic ligands. The coating protects the QDs from oxidation and prevents the leakage of toxic metal ions, especially Cd²⁺, that can induce oxidative burst and programmed cell death (7, 8). In addition, the coat can be used as platform to generate a surface that is biocompatible and amenable to the coupling with biomolecules of interest.

For biological applications, silica coating has several advantages over alternative coating strategies. Because of the high

density of silica, the conjugated particles can be separated easily, during particle preparation and biofunctionalization, from uncoated particles. The silanol groups on the surface decrease hydrophobicity and thus the tendency to agglomerate in aqueous environment. Silica is inert in both aqueous and nonaqueous solvents, which should reduce any noxious effects on the cells hosting the particles as well as microbial degradation (6). Silica coats are tighter against leakage of the toxic Cd²⁺ compared to coats made from SH ligands, such as mercaptoacetic acid, 3-mercaptopropionic acid, 11-mercaptoundecanoic acid, or 2-aminoethanethiol. Furthermore, it is possible to introduce specific surface functionalities by modification of surface hydroxyls with amines, thiols, carboxyls, or methacrylate.

The BSA coating provides better electrostatic colloidal stabilization of QDs in water and is more versatile with respect to active groups (i.e., NH₂, COOH, and SH) for the covalent coupling of antibodies to the BSA-coated QDs. Moreover, the coating of QDs with small proteins produces particles of smaller diameter compared to the SiO₂ approach, which improves their suitability for in vivo imaging.

Biology has entered the so-called postgenomic era, where the assignment of gene to function has become a central task. By the use of reverse genetics, expressed sequences of unknown function are analyzed with respect to phenotypes that occur upon overexpression or suppression of the corresponding gene products and with respect to their intracellular localization. Classical light microscopy and electron microscopy have focussed on the visualization of cellular structures. The so-called functional genomics calls for, in addition, reliable information about the molecular nature of these structures. This requirement has stimulated an impressive bloom of fluorescence microscopy that has developed from an exotic technique used by a handful of specialists into a central tool of molecular biology. There are basically three motive forces that drive this development:

* To whom correspondence should be addressed. Phone: +49 721 608 2144. Fax: +49 721 608 4193. E-mail: peter.nick@bio.uni-karlsruhe.de.

[†] University of Karlsruhe.

[‡] University of Freiburg.

[§] University of East Anglia.

¹ Abbreviations: BSA, bovine serum albumin; BY-2, *Nicotiana tabacum* L. cv. Bright Yellow 2 cell line; FITC, fluorescein isothiocyanate; PBS, phosphate buffered saline; QD, quantum dot.

in vivo imaging, spatial (and temporal) resolution, and molecular specificity. To achieve these goals, the technological progress on the side of microscopical devices has to be complemented by advances on the side of the fluorescent label, and it is this point where the QDs have stimulated enormous interest of cell biologists.

So far, the use of QDs for in vivo imaging has been biased toward studies on the organismic level, for instance, when derivatized QDs were successfully targeted to cancer cells (9, 10) or when they were targeted to the surface of unicellular spores for the detection of the water-borne pathogen *Cryptosporidium* (11). Because of their large size, it is very difficult to exploit the potential of QDs for single-molecule tracking within living cells. Even though it has been published that bona fide labeled kinesins could be tracked in HeLa cells (12), the potential of QDs for spatiotemporal resolution has been mainly demonstrated during in vitro studies on single-molecule tracking (for a recent review see ref 13). For instance, the high bleaching resistance of the QDs made it possible to visualize the hand-over-hand processivity of myosin V during in vitro sliding assays (14).

To conjugate QDs to proteins of interest, in most cases the strong binding of streptavidin (coupled to the QDs) and biotin (coupled to the target protein) is utilized. For instance, in a pioneering work, actin was visualized in cellula through a biotinylated version of phalloidin (an actin-binding compound) that was detected by streptavidin-coupled QDs (15), or microtubules were visualized simultaneously with nuclei through two different streptavidin-coupled QDs that bound to biotinylated secondary antibodies directed against primary antibodies targeted to tubulin and nuclear epitopes (16). A similar approach, where the epitope was visualized by a sandwich composed of three layers (primary antibody, secondary antibody conjugated to biotin, streptavidin-conjugated QDs as tertiary component), was used to visualize chloroplasts in maize leaves in comparison to Alexa 488 as a control fluorophore (17). However, the poor quality of the obtained images and the optical setup used in this experiment indicate that the signal might in fact be due to the autofluorescence of chlorophyll. A general problem of the biotin-streptavidin conjugation is the illegitimate cross-reference between different QD-streptavidin conjugates in dual-visualization experiments. The streptavidin is expected to bind to the biotin on both primary antibodies such that the label will not be attributable to the respective epitope. This problem can be somewhat reduced by sequential labeling; however, the second label will still be partitioned between both epitopes, obscuring the specificity of the label. Especially for the discrimination of closely related epitopes (such as differentially modified subpopulations of a given protein), this will seriously impair the feasibility of this approach.

Thus, the best option to obtain specific labeling would be a direct fluorescence, where the QD label is linked to the primary antibody itself. The pronounced bleaching stability of QDs and their brightness is predicted to yield reasonable signals even in the absence of signal amplification through a secondary antibody (and a tertiary streptavidin conjugate). Streptavidin is a very robust biomolecule that tolerates even massive manipulations without a loss of function. This has been the major reason for the wide use of streptavidin as conjugation partner to introduce QDs into the realm of cell biology. Most proteins are much more delicate with respect to their functionality, and it is a challenging task to couple them with QDs in a nondestructive manner. In a previous work we have coupled silica-coated semiconductor nanocrystals directly to the cytoskeletal protein tubulin and were able to demonstrate the specific self-assembly of the QD-tubulin into fluorescent microtubules (18). In contrast,

antibodies tend to lose their activity when directly coupled to nanoparticles. To date, there is no general solution for coupling biomolecules to nanoparticles under preservation of their biological activity. We therefore ventured to generate biocompatible nanoparticles surfaces that are versatile to be amenable for different kinds of nanoparticles and that are flexible regarding the biological problem. We have chosen two alternative strategies, through a biological surface (bovine serum albumine) and through an inorganic surface (silica), to couple QDs to monoclonal antibodies targeted against tubulin. To challenge the feasibility of this approach for cell-biological applications, we have used the QD-labeled antibodies for direct immunofluorescence following the dynamic reorganization of microtubules during the cell cycle. To our knowledge, this is the first report where QDs have been successfully employed to visualize subcellular details in plant cells.

EXPERIMENTAL PROCEDURES

Synthesis of Luminescent Semiconductor Nanocrystals.

The luminescent CdSe/ZnS NPs were synthesized as described elsewhere (19) and encapsulated in silica using a water-in-oil microemulsion method at room temperature according to our previous protocol (20). Typically, 10 mL of cyclohexane (Roth, Karlsruhe, Germany), 1.3 mL of NP-5 as surfactant (Fluka, Taufkirchen, Germany), and 400 μL of the luminescent CdSe/ZnS NCs (8.72×10^{-7} mol/L) in chloroform (Roth, Karlsruhe, Germany) and 80 μL of tetraethyl orthosilicate (Sigma-Aldrich, Taufkirchen, Germany) as a precursor for silica formation were added in a flask under vigorous stirring. Thirty minutes after formation of the microemulsion, an amount of 150 μL of an aqueous ammonia solution (33 w/v %, Roth, Karlsruhe, Germany) was introduced to initiate the encapsulation process. Subsequently, the reaction mixture was incubated for 24 h at room temperature until completion. Subsequently, the nanoparticles were precipitated from the microemulsion using acetone and were centrifuged and the resultant precipitate of the CdSe/ZnS/SiO₂ composite particles was washed in sequence with butanol, propanol, ethanol (Roth, Karlsruhe, Germany), and water to remove any surfactant and unreacted educts. Finally, the composite particles were dispersed in water. Structure, size, and morphology of the resulting nanoparticles were determined by transmission electron microscopy (TEM; Zeiss LEO 912 Omega operating at 120 kV). For the TEM studies, the specimens were prepared by adding drops of the freshly produced suspension onto a carbon film supported on a Cu grid.

Preparation of Antibody Conjugates with Silica-Shelled Nanocrystals. The silica-encapsulated nanoparticles were briefly spun down, and subjected to three cycles of washing with dry DMSO (Roth, Karlsruhe, Germany), followed by precipitation with dry diethyl ether (Roth, Karlsruhe, Germany). Then, they were redispersed in 1 mL of dry DMSO. A small amount (covering the tip of a spatula) of 1,1'-carbonyldiimidazole (CDI, Fluka, Buchs, Switzerland) was added to the mixture that was then incubated overnight at 4 °C. Subsequently, the nanoparticle dispersion was warmed up to room temperature, incubated for an additional 6 h, and finally centrifuged and resuspended in 1 mL of phosphate buffered saline (PBS). An amount of 200 μL of the primary antibodies at a dilution of 1:10 was added and allowed to bind overnight at 4 °C. The final product was centrifuged and dialyzed against PBS. The resulting conjugates were then used without further purification. As antibodies for the coupling, the mouse monoclonal antibodies DM1A (21) and ATT (22) specific for the α -tubulin subunit were used in this study.

Preparation of Antibody Conjugates with BSA-Coated NPs. The details for preparation and characterization of BSA-coated CdSe/ZnS core-shell particles will be published else-

where (23). Briefly, an amount of 1.5 mL of MeOH was added to 500 μL of CdSe/ZnS nanoparticles in CHCl_3 (8.72×10^{-7} mol/L), and the nanoparticles were isolated by centrifugation. Subsequently, 500 μL of DMSO (Roth, Karlsruhe, Germany) and 10 μL of 2-mercaptoethanol (ME) were added and the sample was heated to 60 °C for 3 h. The nanoparticles were reprecipitated again by addition of 1.3 mL of acetone and 0.2 mL of Et_2O and collected by centrifugation. These hydrophilic nanoparticles were suspended in 500 μL of 2 mg/mL BSA in a Tris-glycine buffer (25 mM Tris, 250 mM glycine, pH 8.3). These BSA-coated nanoparticles were purified by agarose electrophoresis, dialyzed against PBS, and coupled with the target antibodies DM1A and ATT by a standard protocol (24) using *N*-(3-dimethylaminopropyl)-*N'*-ethylcarbodiimide hydrochloride (EDC). The resulting conjugates were used without further purification.

Tobacco Cell Cultures. The tobacco cell line BY-2 (*Nicotiana tabacum* L. cv. Bright Yellow 2 (25)) was cultivated in liquid medium containing 4.3 g/L Murashige and Skoog salts (Duchefa, Haarlem, The Netherlands), 30 g/L sucrose, 200 mg/L KH_2PO_4 , 100 mg/L inositol, 1 mg/L thiamine, and 0.2 mg/L 2,4-dichlorophenoxyacetic acid (2,4-D), pH 5.8. Cells were subcultured weekly, inoculating 1.5–2 mL of stationary cells into 30 mL of fresh medium in 100 mL Erlenmeyer flasks. The cell suspensions were incubated at 25 °C in the dark on an orbital shaker (KS250 basic, IKA Labortechnik, Staufen, Germany) at 150 rpm. Stock BY-2 calli were maintained on media solidified with 0.8% (w/v) agar and subcultured monthly. All experiments were performed 4 days after subcultivation.

Visualization of Microtubules by Indirect Immunofluorescence Using FITC as Label. Microtubules were processed for immunofluorescence in self-made staining chambers using a nylon mesh of 70 μm pore width as published previously (26). This allowed fast exchange of media at preventing the loss of cells during the staining. After fixation for 30 min with 3.7% (w/v) paraformaldehyde in microtubule stabilizing buffer (MSB: 50 mM PIPES, 2 mM EGTA, 2 mM MgSO_4 , 0.1% Triton X-100, pH 6.9), cells were washed in PBS three times for at least 5 min to remove excess paraformaldehyde. Subsequently, the cell wall was digested using 1% (w/v) Macerozyme (Duchefa, Haarlem, The Netherlands) and 0.2% (w/v) Pectolyase (Fluka, Taufkirchen, Germany) in MSB for 5 min. Again, excess enzyme was washed out for 5 min with PBS. Unspecific binding sites were blocked for 20 min with 0.5% (w/v) BSA diluted in PBS. Directly after blocking, the cells were transferred into a small volume of the primary antibody. To visualize microtubules, we used a 1:250 dilution in PBS of either DM1A recognizing a conservative epitope near the carboxyterminus of α -tubulin (21) or ATT recognizing the carboxyterminal 12 amino acid residues of full-length α -tubulin (22), both purchased from Sigma (Taufkirchen, Germany). This primary antibody was allowed to bind overnight at 4 °C. The next day, unbound primary antibody was removed by washing the cells three times for at least 5 min in PBS. The sample was then incubated with a secondary FITC-conjugated antibody targeted against mouse IgG for 1 h at 37 °C in a moist chamber to prevent drying of the specimen. Unbound secondary antibody was removed by washing with PBS, and DNA was stained using 0.1 $\mu\text{g mL}^{-1}$ Hoechst 33258 (2'-(4-hydroxyphenyl)-5-(4-methyl-1-piperazinyl)-2,5'-bi-1*H*-benzimidazole trihydrochloride hydrate) (Sigma, Taufkirchen, Germany).

Visualization of Microtubules by Direct Immunofluorescence Using QDs as Label. The cells were fixed, digested with Macerozyme, blocked, and washed as described above. After the unspecific binding sites were blocked, the cells were incubated overnight at 4 °C with the primary monoclonal

antibody against α -tubulin that had been coupled to biofunctionalized, fluorescent CdSe-based semiconductor nanocrystals. The antibody–NC conjugates were adjusted with PBS to a dilution of 1:250 as used in the indirect FITC-based immunofluorescence described above. After unbound particles were washed out the next day, the sample was directly used for the staining of DNA by Hoechst 33258 as described above. To assess the success of bioconjugation for each antibody–NC conjugate batch, a specimen processed in parallel was post-stained with a secondary FITC-conjugated antmouse IgG for 1 h at 37 °C and then triple-stained with Hoechst 33258.

Microscopy and Image Analysis. The samples were examined under an AxioImager Z.1 microscope (Zeiss, Jena, Germany) equipped with an ApoTome microscope slider for optical sectioning and a cooled digital CCD camera (AxioCam MRm). For the observation of the QD-antibody conjugates, the filter set 43 HE (excitation at 550 nm, beamsplitter at 570 nm, and emission at 605 nm) was used. The DNA signal and the FITC fluorescence were viewed through filter sets 49 (excitation at 365 nm, beamsplitter at 395 nm, and emission at 445 nm) and 38 HE (excitation at 470 nm, beamsplitter at 495 nm, and emission at 525 nm) (Zeiss, Jena, Germany). A test for potential filter cross-talk, where single-stained samples were viewed with the three filter sets at corresponding exposure conditions, revealed that the filters were tight for the three fluorochromes (data not shown). The images were analyzed using the Axio-Vision (release 4.5) software and processed for publication using Photoshop (Adobe Systems, San Jose, CA).

RESULTS AND DISCUSSION

Synthesis of CdSe-Based NPs and Their Antibody Conjugates. We used two strategies to prepare the antibody conjugates, which are presented in parts a and b of Figure 1. In the first one the water solubility of NPs has resulted from encapsulation with the hydrophilic SiO_2 layer and the free OH groups on the surface have been used for conjugation of the NPs with tubulin antibody ATT or DM1A via a CDI cross-linker.

In the first strategy (Figure 1a), the CdSe/ZnS nanocrystals were transferred into water by a standard ligand exchange method utilizing 2-mercaptoethanol (ME). In the next step, the product was coated with bovine serum albumine (BSA) to stabilize the nanoparticles against coagulation in water and to provide free chemical groups for improved covalent conjugation (23). The covalent coupling between BSA and the antibodies DM1A and ATT occurred via the standard reagent EDC through mutual coupling between free carboxylic and amino side groups on the two respective proteins. The detailed characterization of these particles will be published elsewhere (23).

The second strategy (Figure 1b) was based on silica coating as published previously (20). Transmission electron micrographs from the resulting CdSe/ZnS nanoparticles and their silica-coated nanocomposites are shown in parts a and b of Figure 2, respectively. Since the electron density of the CdSe/ZnS core is significantly higher than that of silica, the darker and lighter parts of the particles in Figure 2b correspond to the CdSe/ZnS core and the silica shell, respectively. The size distributions of the CdSe/ZnS core particles (Figure 3a), and the CdSe/ZnS/ SiO_2 nanocomposites (Figure 3b) were calculated from the micrograph over several hundred individuals. The average diameter of the CdSe/ZnS core particles was 5.8 nm, and the diameter of the silica-coated nanoparticles was 41.6 nm.

The particles obtained by the two approaches were coupled to the monoclonal antitubulin antibodies ATT and DM1A as described in detail in Experimental Procedures. Because of the high affinity and specificity of these antibodies, they are used at highly diluted preparations such that it was not feasible to

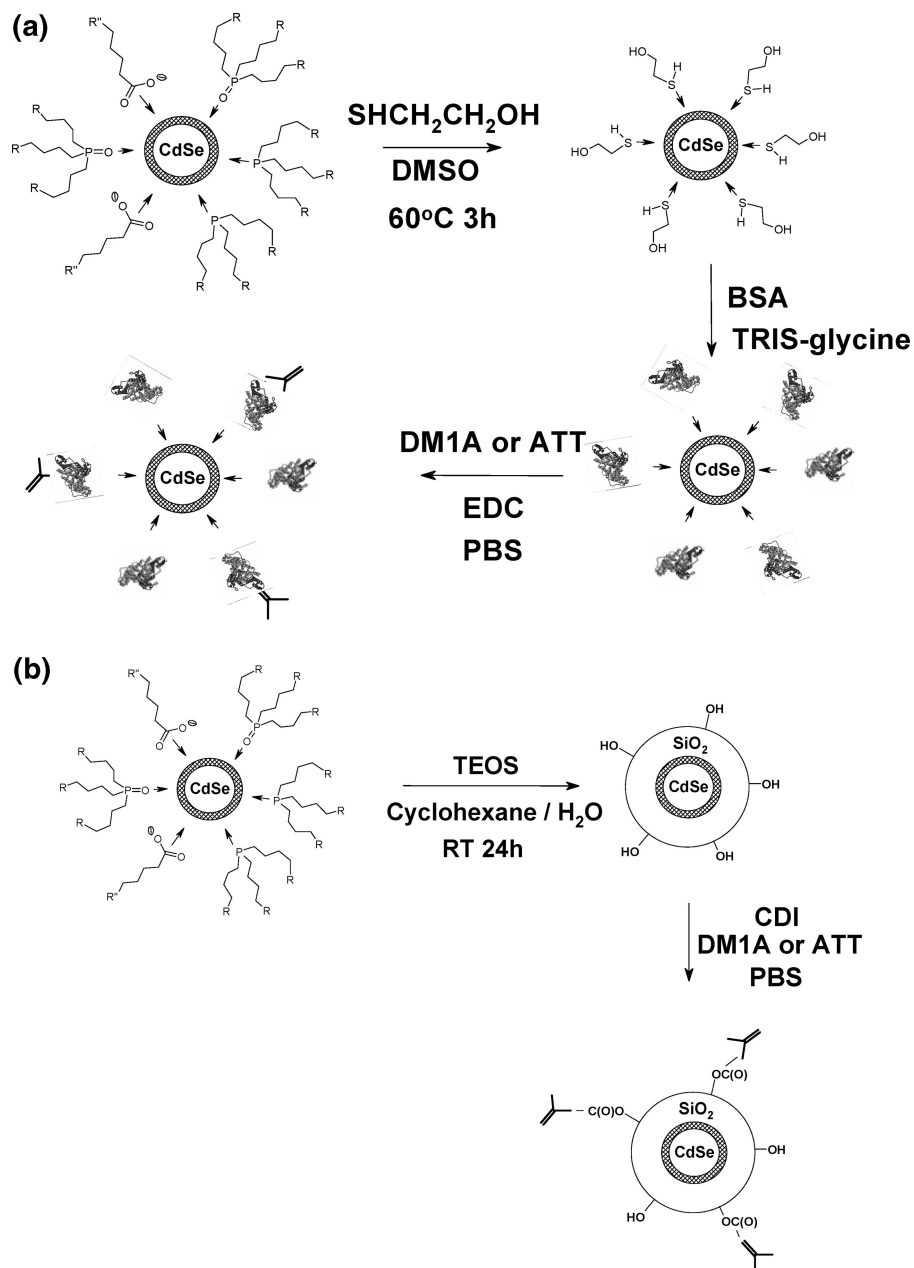


Figure 1. Strategies to conjugate fluorescent CdSe semiconductor nanocrystals to monoclonal antibodies: (a) coupling through coating with bovine serum albumine; (b) coupling through coating with a silica shell with surface functionalities. The black layer around the CdSe core crystal stands for the ZnS shell.

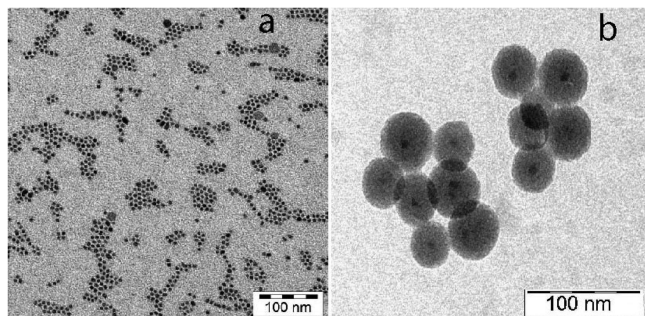


Figure 2. Transmission electron micrographs of (a) the CdSe/ZnS core nanoparticles and (b) the CdSe/ZnS/SiO₂ nanoparticles.

characterize the conjugates by electron microscopy or any other method, such as gel electrophoresis, dynamic light scattering, or size exclusion chromatography. To assess the success of the

bioconjugation, we therefore tested the biological functionality (i.e., the immunofluorescence in the target cells) as indicator.

Tubulin Antibodies Conjugated to BSA-Coated Nanocrystals Decorate Microtubules. As the first approach, antibodies conjugated to biofunctionalized, BSA-shelled nanocrystals were used for direct immunofluorescence of microtubules in the tobacco cell line BY-2 (Figure 4). These cells divide readily in suspension culture and are endowed with a clear axis and polarity, which allows very clear identification of the various microtubular arrays that form during the cell cycle.

In premitotic interphase cells, the antitubulin-NC conjugates visualize punctate signals in the cell periphery that are aligned perpendicular to the main axis of the cell file (Figure 4A). This specific orientation, the general appearance, and the localization in the cortical cytoplasm show that these structures correspond to the cortical microtubules typical for this stage of the cell cycle. When confocal sections are recorded from the cell center (parts B1 and B2 of Figure 4), the nanocrystal signal is observed

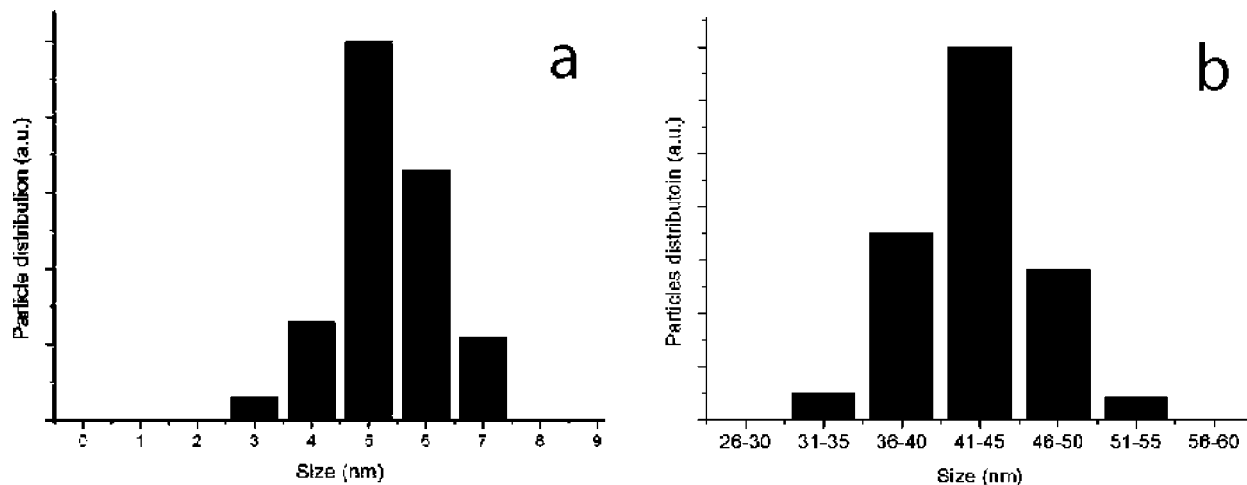


Figure 3. Frequency distribution over particle size for (a) the CdSe/ZnS core particles and (b) the CdSe/ZnS/SiO₂ nanoparticles based on scores of transmission electron micrographs from several hundred individual particles.

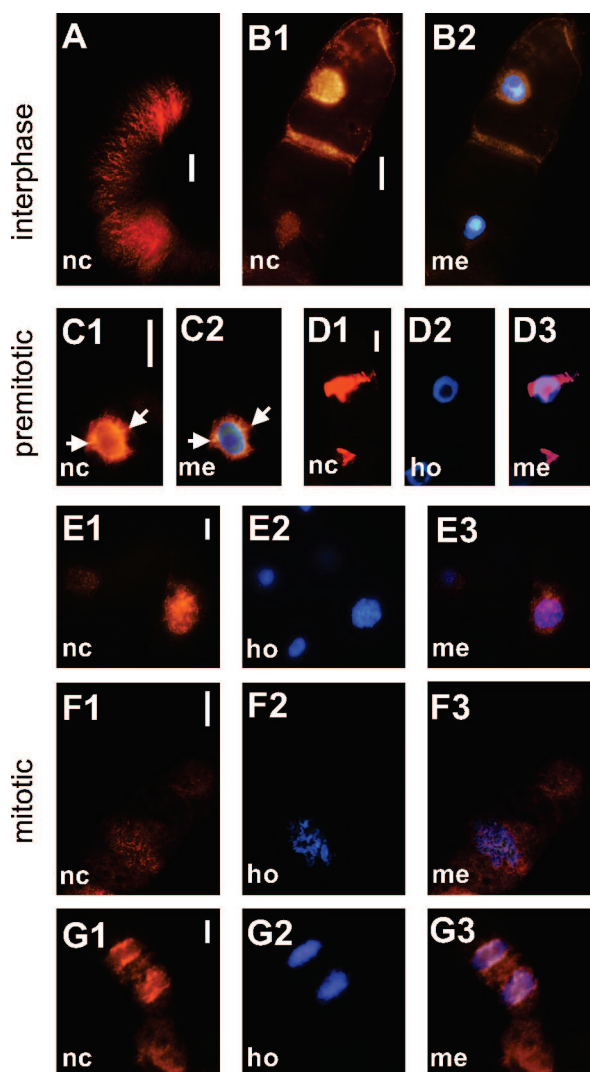


Figure 4. Direct immunofluorescence of tubulin with monoclonal mouse antitubulin antibodies conjugated to BSA-coated QDs followed through different stages of division in tobacco BY-2 cells: (nc) optical setup for the detection of nanocrystals; (ho) optical setup for the detection of DNA (through Hoechst 33258); (me) merge of the two channels to show the QD signal in relation to the DNA. Size of bar is 10 μ m.

at the nuclear envelope that ensheathes the DNA. The nuclear envelope is the major microtubule-organizing center in the

acentriolar cells of higher plants, and therefore, this nanocrystal signal corresponds to the microtubule-organizing centers that decorate the nuclear surface of plant cells.

Cell division is heralded by a movement of the nucleus into the cell center to the prospective division site and the formation of a microtubular preprophase band from the nuclear envelope that predicts position and orientation of the future cross wall. Both the nuclear envelope (parts C1 and C2 of Figure 4) and the preprophase band that progressively emerges from the nuclear envelope (white arrows in parts C1 and C2 of Figure 4) until a massive band of microtubules is produced (parts D1–D3 of Figure 4) are decorated by the nanocrystal signal.

During the mitotic prophase, when the DNA is condensed into chromosomes (part E2 of Figure 4), the nuclear envelope collapses and the nanocrystals are found to surround the forming spindle (parts E1 and E3 of Figure 4). In the following metaphase, the nanocrystal signal will then attach to the chromosomes spread in the equatorial cell plane (parts F1–F3 of Figure 4) and redistribute to the newly reestablished nuclear envelopes of the daughter nuclei and at the newly forming cross wall in the final telophase (parts G1–G3 of Figure 4).

Thus, the distribution of the nanocrystal–antibody conjugates mirrors exactly the behavior of the microtubular cytoskeleton during the cell cycle. However, the signal obtained by this approach was never contiguous but remained punctate.

As to testing whether the punctate nanocrystal signal was in fact colocalizing with microtubules or whether it was produced by disintegration of microtubules, we counterstained the samples with a FITC-conjugated secondary antibody raised against the primary antitubulin antibody. By dual-channel visualization of the nanocrystal and the FITC signal, it was thus possible to see the context of the nanocrystals with microtubules (Figure 5). To check for a potential filter leakage of the FITC signal upon the nanocrystal signal, we viewed cells, where microtubules had been visualized by a primary antibody that was not conjugated to nanocrystals, as a negative control. When these cells were incubated with the FITC-conjugated secondary antibody (part A1 of Figure 5) and then viewed with the filter used to record the nanocrystal signal, the result was clearly negative (part A1 of Figure 5), demonstrating that the optical setup was tight enough to separate the FITC signal and the nanocrystal signal in dual-channel configurations.

We therefore followed the cell cycle of tobacco cells using triple staining (nanocrystal–antitubulin antibodies, FITC, and Hoechst 33258 for the visualization of DNA). In interphase cells (parts B1–B4 of Figure 5), the cortical microtubules visualized by the secondary antibody (part B2 of Figure 5) were found to

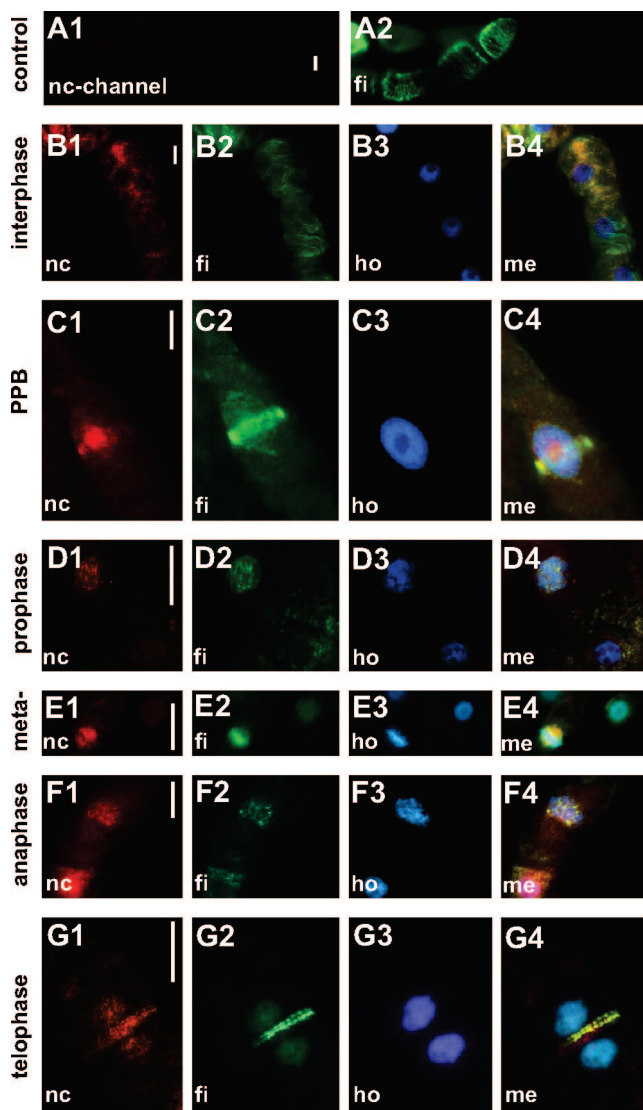


Figure 5. Direct immunofluorescence of tubulin with monoclonal mouse antitubulin antibodies conjugated to BSA-coated QDs and after-staining with FITC-conjugated antimouse IgG followed through different stages of division in tobacco BY-2 cells: (nc) optical setup for the detection of nanocrystals; (fi) optical setup for the detection of the FITC after stain; (ho) optical setup for the detection of DNA (through Hoechst 33258); (me) merge of the three channels to show the QD signal in relation to microtubules and DNA. Size of bar is 10 μm . Parts A1 and A2 show the negative control using unconjugated primary antibody and after stain with FITC-conjugating antimouse IgG (i.e., omitting the QD-conjugated antibodies) to test for potential optical cross-contamination of the nc optical setup through the FITC signal. The negative results show that the optical setup is tight against filter leakage.

be decorated with the nanocrystal signal (part B1 of Figure 5). The merged image exhibited numerous yellow microtubules indicating the high congruence of both signals (part B4 of Figure 5). This congruence was maintained when the cells were prepared for mitosis and generated a preprophase band (parts C1–C4 of Figure 5). Also, the various microtubular arrays characteristic for mitosis such as the nuclear cap in the late prophase (parts D1–D4 of Figure 5), the division spindle in metaphase (parts E1–E4 of Figure 5), and the exploratory microtubules formed at anaphase (parts F1–F4 of Figure 5) were correctly depicted by the two signals. When the microtubular phragmoplast in the late telophase is formed (parts G1–G4 of Figure 5), the nanocrystals decorate the complete region where FITC-labeled microtubules are seen. In addition, the nanocrystal conjugates can be detected in the adjacent cytoplasm and already

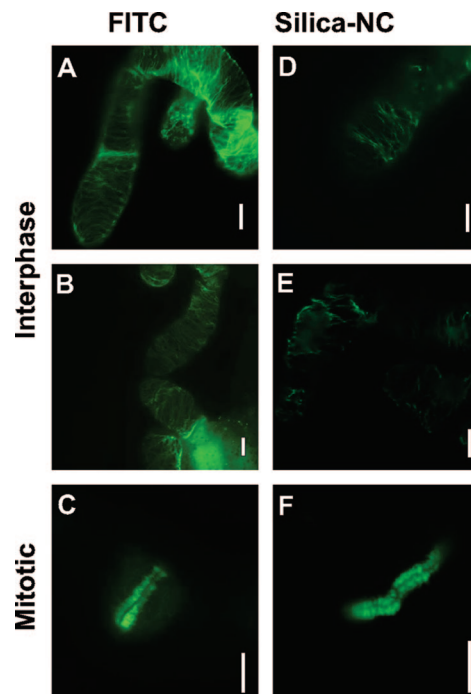


Figure 6. Direct immunofluorescence of tubulin with monoclonal antitubulin antibodies conjugated to silica-coated QDs (D–F) in comparison to the signal obtained by conventional indirect immunofluorescence using secondary antibodies conjugated to FITC (A–C) followed through different stages of division in tobacco BY-2 cells. Size of bar is 10 μm . The two labels are equivalent in terms of specificity, signal-to-noise ratio, intensity, and structural preservation.

very clearly at the nuclear surface of the daughter nuclei (part G1 of Figure 5), where the FITC signal is much weaker (part G2 of Figure 5).

Thus, upon counterstaining with a FITC-conjugated secondary antibody and dual visualization of both signals, the entire dynamics of microtubule arrays characteristic for the plant-cell cycle can be reliably followed. The punctate staining seen for the nanocrystal–antibody conjugates (Figure 4) is therefore not due to microtubules that had been disrupted by the incubation with the nanocrystal–antibody conjugates. Microtubules have remained intact during the labeling procedure and can be contiguously stained by a FITC-conjugated secondary antibody. This indicates that the affinity of the nanocrystal–antibody conjugate for tubulin has been preserved as well as the specificity of binding. However, either a significant proportion of the antitubulin antibody is not conjugated with the nanocrystals or the fluorescence has been lost during the conjugation. These unlabeled primary mouse antibodies are still functional and bind to their cellular target but will not display the fluorescent signal. They can be rendered visible, however, by addition of an antimouse IgG secondary antibody coupled to FITC.

Tubulin Antibodies Conjugated to Silica-Shelled Nanocrystals Label Microtubules. To obtain a contiguous microtubule signal, we therefore tested an alternative approach for the conjugation of the nanocrystals to antitubulin antibodies. The nanocrystals were surrounded by a silica shell that was coated with functional groups that could be used for coupling (20). These silica-shelled nanocrystals were then conjugated with antitubulin antibodies and used for direct immunofluorescence in both interphase and mitotic cells of tobacco BY-2 (Figure 6). Conventional labeling of microtubules by indirect immunofluorescence using FITC (parts A–C of Figure 6) was performed in comparison, and both the cortical microtubules (parts A and

B of Figure 6) and mitotic arrays such as the phragmoplasts that organize the new cell plate after completed segregation of the daughter nuclei (part C of Figure 6) were visualized. The silica-shelled nanocrystals (parts D–F of Figure 6) produced a contiguous microtubule signal by direct immunofluorescence that was equivalent, in both the signal amplitude and morphology, to the signal of the conventional label. This signal was now contiguous for both the cortical microtubules (parts D and E of Figure 6) and the phragmoplast (part F of Figure 6) at a simultaneously very low background signal. Thus, the result obtained for the silica-shelled nanocrystals was equivalent to the conventional indirect immunofluorescence.

To summarize our results, we state that both approaches were successful in visualizing the specific epitopes of the antitubulin antibodies through QD-based direct immunofluorescence. However, the conjugation in the BSA-coating approach seemed to be only partial, whereas the SiO₂-coat approach produced a more complete conjugation. This difference might be due to the considerably larger surface of the silica-coated particles at the same concentration of the core CdSe/ZnS Qds. The functionality of the tubulin antibody was maintained in both cases; this is also seen in the FITC-afterstain experiment (Figure 5), where the unconjugated tubulin antibodies were stained by the FITC-labeled secondary antibody and found to be perfectly aligned with microtubules. The signal strengths obtained with direct immunofluorescence using the QDs were absolutely comparable to those resulting from conventional indirect immunofluorescence (Figure 6). Given the fact that up to 50 secondary antibodies bind to one primary antibody in the conventional indirect immunofluorescence, one has to conclude that the fluorescence intensity produced by an individual QD-conjugated antibody is very high.

OUTLOOK

Functional genomics is increasingly extending into the analysis of differentially modified subpopulations of a given protein in order to understand the spatiotemporal dynamics and cell biological function of these modifications (26). Double visualization of such subpopulations using highly specific monoclonal antibodies is so far impaired by the fact that these antibodies are almost exclusively available from one animal species (mouse). It is extremely difficult to safeguard against illegitimate cross-reaction of the secondary fluorescent antisera. Direct immunofluorescence would be a good alternative but is limited by low signal strength because the signal amplification due to the labeled secondary antibody is lacking. We could demonstrate in our study that this limitation can be overcome by direct coupling of fluorescent QDs to highly specific antisera while preserving functionality and specificity of the antibody. This should now allow, for instance, visualization of different modifications on the tubulin on the same microtubule. By use of QDs with specific optical properties (such as delayed photostimulated luminescence), it should be possible to obtain higher levels of specificity and better spatiotemporal resolution in confocal applications because a higher number of individual scans can be averaged to increase signal/noise ratios and input amplifications (possible reduced noise/signal ratios). We have demonstrated for the first time that QDs can be successfully utilized in intact, unsectioned plant cells despite the presence of a massive cellulosic cell wall. In the next step we want to extend the use of QDs to the *in vivo* situation by mild and transient permeabilization of the plasma membrane without infringing viability. In this context it is mainly size that matters such that the BSA-coated particles with their considerably smaller size might become crucial. By use of nanoparticles that are magnetic, it should become possible not only to visualize but also to manipulate specific cellular targets in living plant cells.

ACKNOWLEDGMENT

This work was supported by the Research Priority Programme of the State of Baden-Württemberg (Project LuNaCell) to T.N. and P.N. and by the Center for Functional Nanoscience of the University of Karlsruhe (Project E1.5) to P.N. The authors thank Dr. Jürgen Riegler and Dr. Ralf Thomann for preparation of the CdSe/ZnS nanoparticles and for TEM measurements, respectively. Sabine Purper is acknowledged for the technical assistance in the culture of tobacco cells.

LITERATURE CITED

- (1) Michalet, X., Pinaud, F. F., Bentolila, L. A., Tsay, J. M., Doose, S., Li, J. J., Sundaresan, G., Wu, A. M., Gambhir, S. S., and Weiss, S. (2005) Quantum dots for live cells, *in vivo* imaging, and diagnostics. *Science* 307, 538–544.
- (2) Medintz, I. L., Uyeda, H. T., Goldman, E. R., and Mattoussi, H. (2005) Quantum dot bioconjugates for imaging, labelling and sensing. *Nat. Mater.* 4, 435–446.
- (3) Chen, F., and Gerion, D. (2004) Fluorescent CdSe/ZnS nanocrystal-peptide conjugates for long-term, nontoxic imaging and nuclear targeting in living cells. *Nano Lett.* 4, 1827–1832.
- (4) Shibahara, A., Hoshino, A., Hanaki, K. I., Suzuki, K., and Yamamoto, K. (2004) On the cyto-toxicity caused by quantum dots. *Microbiol. Immunol.* 48, 669–675.
- (5) Kirchner, C., Liedl, T., Kudera, S., Pellegrino, T., Javier, A. M., Gaub, H. E., Stölzle, S., Fertig, N., and Parak, W. J. (2005) Cytotoxicity of colloidal CdSe and CdSe/ZnS nanoparticles. *Nano Lett.* 5, 331–338.
- (6) Zhang, T., Stilwell, J. L., Gerion, D., Ding, L., Elboudwarej, O., Cooke, P. A., Gray, J. W., Alivisatos, A. P., and Chen, F. F. (2006) Cellular effect of high doses of silica-coated quantum dot profiled with high throughput gene expression analysis and high content cellomics measurements. *Nano Lett.* 6, 800–808.
- (7) Rikans, L. E., and Yamano, T. J. (2000) Mechanisms of cadmium-mediated acute hepatotoxicity. *Biochem. Mol. Toxicol.* 14, 110–117.
- (8) Schützendübel, A., and Polle, A. (2002) Plant responses to abiotic stresses: heavy metal-induced oxidative stress and protection by mycorrhization. *J. Exp. Bot.* 53, 1351–1365.
- (9) Gao, X., Cui, Y., Levenson, R. M., Chung, L. W. K., and Niel, Sh. (2004) *In vivo* cancer targeting and imaging with semiconductor quantum dots. *Nat. Biotechnol.* 22, 969–976.
- (10) Yu, X., Chen, L., Li, K., Li, Y., Luo, S. X., Liu, J., Deng, L. Z. Y., Pang, D., and Wang, Q. (2007) Immunofluorescence detection with quantum dot bioconjugates for hepatoma *in vivo*. *J. Biomed. Opt.* 12, 014008.
- (11) Lee, L. Y., Ong, S. L., Hu, J. Y., Ng, W. J., Feng, Y., Tan, X., and Wong, S. W. (2004) Use of semiconductor quantum dots for photostable immunofluorescence labeling of *Cryptosporidium parvum*. *Appl. Environ. Microbiol.* 70, 5732–5736.
- (12) Courty, S., Luccardini, C., Bellaiche, Y., Cappello, G., and Dahan, M. (2006) Tracking individual kinesin motors in living cells using single quantum-dot imaging. *Nano Lett.* 6, 1491–1495.
- (13) Jaiswal, J. K., and Simon, S. M. (2007) Imaging single events at the cell membrane. *Nat. Chem. Biol.* 3, 92–98.
- (14) Warshaw, D. M., Kennedy, G. G., Work, S. S., Kremensova, E. B., Beck, S., and Trybus, K. M. (2005) Differential labeling of myosin V heads with quantum dots allows direct visualization of hand-over-hand processivity. *Biophys. J.* 88, L30–L32.
- (15) Bruchez, M., Moronne, M., Gin, P., Weiss, Sh., and Alivisatos, A. P. (1998) Semiconductor nanocrystals as fluorescent biological labels. *Science* 281, 2013–2016.
- (16) Wu, X., Liu, H., Liu, J., Haley, K. N., Treadway, J. A., Larson, J. P., Ge, N., Peale, F., and Bruchez, M. P. (2002) Immunofluorescent labeling of cancer marker Her2 and other cellular targets with semiconductor quantum dots. *Nat. Biotechnol.* 21, 41–46.

- (17) Müller, F., Houben, A., Barker, P. E., Xiao, Y., Käs, J. A., and Melzer, M. (2006) Quantum dots—a versatile tool in plant science? *J. Nanobiotechnol.* *4*, 5–10.
- (18) Riegler, J., Nick, P., Kielmann, U., and Nann, T. (2003) Visualize the self-assembly of tubulin with luminescent nanorods. *J. Nanosci. Nanotechnol.* *3*, 380–385.
- (19) Ziegler, J., Merkulov, A., Grabolle, M., Resch, U., and Nann, T. High quality ZnS shells for CdSe nanoparticles—a rapid, low toxic microwave synthesis. *Langmuir*, in press.
- (20) Darbandi, M., and Nann, T. (2005) Single quantum dots in silica spheres by microemulsion synthesis. *Chem. Mater.* *17*, 5720–5725.
- (21) Breitling, F., and Little, M. (1986) Carboxy-terminal regions on the surface of tubulin and microtubules. Epitope locations of YOL1/34, DM1A and DM1B. *J. Mol. Biol.* *189*, 367–370.
- (22) Kreis, T. E. (1987) Microtubules containing de-tyrosinylated tubulin are less dynamic. *EMBO J.* *6*, 2597–2606.
- (23) Bücking, W., Merkulov, A., and Nann, T. Manuscript in preparation.
- (24) Hermanson, G. T. (1996) *Bioconjugate Techniques* p 785, Academic Press, New York.
- (25) Nagata, T., Nemoto, Y., and Hasezawa, S. (1992) Tobacco BY-2 cell line as the “Hela” cell in the cell biology of higher plants. *Int. Rev. Cytol.* *132*, 1–30.
- (26) Nick, P., Heuing, A., and Ehmann, B. (2000) Plant chaperonins: a role in microtubule-dependent wall-formation? *Protoplasma* *211*, 234–244.
- (27) Wiesler, B., Wang, Q.Y., and Nick, P. (2002) The stability of cortical microtubules depends on their orientation. *Plant J.* *32*, 1023–1032.

BC700188D